Supporting Information for "Impact of vertical mixing parameterizations on internal gravity wave spectra in regional ocean models"

Ritabrata Thakur[1], Brian K. Arbic[1], Dimitris Menemenlis[2], Kayhan

Momeni[3], Yulin Pan[4], W. R. Peltier[3], Joseph Skitka[1], Matthew H. Alford[5],

Yuchen Ma[3]

[1]Department of Earth and Environmental Sciences, University of Michigan, Ann Arbor, MI, USA

[2]Jet Propulsion Laboratory, California Institute of Technology, Pasadena, CA, USA

[3]Department of Physics, University of Toronto, Toronto, Canada

[4]Department of Naval Architecture and Marine Engineering, University of Michigan, Ann Arbor, MI, USA

[5]Scripps Institution of Oceanography, University of California San Diego, La Jolla, CA, USA

In this supporting information (SI) section, we first describe the details of the ocean simulations in section 1. We then describe the methodology of calculating "WKBJ-stretched" depths in section 2 and the methodology of computing vertical wave-number spectra in section 3. We discuss the model resolution and the resolved internal wave field in section 4.

————

Corresponding author: Ritabrata Thakur. Suite 2534, Department of Earth and Environmental Sciences, University of Michigan, Ann Arbor, MI 48109, USA. (ritabrata90official@gmail.com)

July 16, 2022, 11:13am

The vertical level thicknesses of the simulations are shown in Fig S1 and the relationship between actual ocean depth and the WKBJ-stretched depth is in Fig S2. We show the sensitivity of the kinetic energy (KE) spectra at three different vertical resolutions of the model to the background mixing components of the K-Profile Parameterization (KPP) by comparing them with the KE spectra from McLane moored profilers (MP) in Fig S3. The effect of KPP background components in different frequency bands of the modeled KE spectra for the 264-level simulation is seen in Fig S4 where we see that in all the frequency bands, the modeled KE spectra with the KPP background turned off have a higher variance in the IW continuum. We find that the deep ocean (1500–4000 m) modeled KE spectra are sensitive to model vertical resolution as they progressively include more variance in the IW continuum with an increase in model vertical resolution (Fig S5). In S6, the ratios of modeled strain to MP strain in different frequency bands show that the model always has lower high-wavenumber strain. In Fig S7, we show the deep ocean (1500–4000 m) modeled strain spectra and see improvement in strain variance with an increase in model resolution. In Fig S8, we discuss the resolved internal wave scales in the 264-level simulation when compared to the full ocean internal wave field.

1.   Global and regional simulations

The numerical simulations in this study were carried out using a hydrostatic configuration of the Massachusetts Institute of Technology general circulation model (MITgcm; Marshall, Adcroft, Hill, Perelman, and Heisey (1997); Adcroft et al. (2018)). The global simulation which forces the regional simulations in this paper has previously been referred to as LLC4320 (Rocha et al., 2016) and MITgcm48 (Savage et al., 2017). This global sim-

ulation has a horizontal grid spacing of $1/48°$ (~ 2 km in the simulation domain) and 90 vertical levels with a surface level thickness of 1m which progressively increases with depth to a maximum thickness of 480m (Fig S1). The model depth is approximately 6 km in the deepest parts of the domain. The LLC4320 simulation uses a Latitude-Longitude-polar Cap (LLC) horizontal grid configuration and includes a dynamic/thermodynamic sea ice model (Losch et al., 2010). A progressive spin-up strategy was employed, starting from a data-constrained, $1/6°$ simulation (Menemenlis et al., 2008) and progressing through a 1-year simulation at $1/12°$ and an 8-month simulation at $1/24°$. The integration time step for the LLC4320 simulation is 25 s. For our purposes, we use hourly snapshots of the model output. The model setup of the global LLC4320 simulation can be found at `http://mitgcm.org/viewvc/MITgcm/MITgcm_contrib/llc_hires` and the model output at `https://data.nas.nasa.gov/ecco/`.

The regional simulations in this paper have three different vertical grid spacings (see Fig S1), while the horizontal grid spacing is identical to that of the global LLC4320 simulation. The regional simulations begin on 1 March 2012 with the initial state from LLC4320 interpolated onto the requisite vertical grid. These simulations are forced by realistic atmospheric and astronomical tidal forcing (Arbic et al., 2018). The wind and other surface variables like temperature and humidity are updated on a 6-hourly basis from $0.14°$ European Center for Medium-Range Weather Forecasts (ECMWF) analysis starting in 2011. The atmospheric fields are converted to surface fluxes using the bulk formulae of Large and Yeager (2004). At every model time step, a hard boundary condition without the use of a sponge layer is enforced at the lateral boundaries of the regional model to

match the fields of the regional simulation to that of the global LLC4320 simulation. The horizontal mixing is prescribed based on the modified Leith scheme of Fox-Kemper and Menemenlis (2008) and the vertical mixing by the K-Profile Parameterization (KPP) of Large, McWilliams, and Doney (1994). The model uses the ocean bathymetry of Smith and Sandwell (1997). With a change in the vertical level thicknesses of the regional simulations, the integration time step also need to be adjusted. The highest vertical resolution (264-level) simulation has a time step of 10 s, the 153-level simulation uses 15 s, and the lowest vertical resolution (109-level) simulation was run with a time step of 25 s, the latter being the same as the global LLC4320 time step. We use hourly snapshots of model output from these regional simulations in all of our analyses. The regional simulation output and the analysis codes can be found at `https://doi.org/10.7910/DVN/HOVAPO`.

2.   WKBJ-stretched depths

Internal wave propagation is affected by changes in ocean stratification. To account for the effect of variable stratification in computing the vertical wavenumber spectra, both velocity and depths from model and MP observations need to be normalised by the buoyancy frequency. The horizontal velocities are scaled by $(\overline{\mathrm{N}}(z)/\mathrm{N}_0)^{1/2}$, where $\mathrm{N}(z)$ is the Brunt–Väisälä frequency with the overbar denoting time average for the model run time or the MP deployment time, and the constant $\mathrm{N}_0 = 3$ cph following Leaman and Sanford (1975). The "WKBJ-stretched" or buoyancy-frequency-stretched depths (z_s) are estimated according to the differential equation $dz_s = (\overline{\mathrm{N}}(z)/\mathrm{N}_0)dz$. The vertical wavenumbers are then $1/\Delta z_s$ in units of cycles per stretched-meter (cpm). An example

relationship between the actual ocean depths and the stretched depths for the 264-level model is shown in Fig S2 (a) and the buoyancy frequency profile used for scaling is shown in Fig S2 (b). The vertical wavenumber spectra presented in this paper are based on the stretched depths.

3. Spectral estimates

The vertical wavenumber spectra are calculated as time averages of individual one-dimensional spectra of the fields in the vertical direction. For the simulations, the spectra are averaged over approximately 73 days of model runs and for the deployment days of the MPs. The means and linear trends are removed from the model output and MP data before spectra calculations. A Hanning window is used to taper the velocities, temperature, and salinity at the vertical ends of the water column for all the spectral calculations. The reduced variances due to this tapering are added back into the spectral estimates. Ocean vertical velocities are generally smaller than horizontal velocities and hence not included here due to greater uncertainties in their measurements. Due to the relatively low number of grid points in the vertical direction (40 points for the 109-level and 58 points for the 264-level model in the 80–1400 m depth range), we use the whole water column to calculate the spectra for both model and MP, i.e., there is no segmenting of the velocities and scalar field involved unlike that used in traditional frequency spectra calculation using overlapping segments (e.g., the Welch periodogram method (Welch, 1967)). The highpass and the lowpass definition used in this paper have a cutoff of 11.5 hr and are hence the supertidal and subtidal frequency bands. The near-inertial band is

90–110% of the local inertial period at each MP location. The inertial period is 27.84 hr at MP1 and 23.92 hr at MP4.

4. A note on resolved internal wave field

The approximate wavenumber bounds of the ocean internal wave field are shown in Fig S8. Lines of constant internal wave frequencies ω are drawn using the dispersion relation $\omega^2 = (f^2 m^2 + \mathrm{N}^2 k^2)/(k^2 + m^2)$, where f is the inertial period at 30° N, N = N_0 = 3 cph, k are the horizontal wavenumbers, and m are the stretched vertical wavenumbers. The red rectangle in Fig S8 shows the scales resolved by the 264-level simulations.

The modeled highpass shear is low in variance for vertical wavenumbers greater than 0.007–0.008 cpm (Fig 3 (h)) and is more than an order of magnitude lower than the observations at the highest resolvable wavenumber. Fig S8 shows that for vertical wavenumbers higher than, say, 0.007–0.008 cpm, the model captures only a small portion of the highpass band (the area between the orange line and the red rectangle above vertical wavenumber 0.007 cpm). This limitation in model horizontal resolution could be responsible for the reduced variance in the modeled highpass shear and probably also for high wavenumber strain. Future simulations will include finer horizontal resolution aimed towards resolving the smallest internal wave scales, although this will be extremely expensive in terms of computational cost and data storage.

References

Adcroft, A., Campin, J.-M., Doddridge, S. D., Evangelinos, C., Ferreira, D., Follows, M., ... others (2018). Mitgcm documentation. *Release checkpoint67a-12-gbf23121*, *19*. Retrieved from `https://buildmedia.readthedocs.org/media/pdf/mitgcm/`

`latest/mitgcm.pdf` (Accessed: 12-29-2021)

Arbic, B. K., Alford, M. H., Ansong, J. K., Buijsman, M. C., Ciotti, R. B., Farrar, J. T., . . . others (2018). A primer on global internal tide and internal gravity wave continuum modeling in HYCOM and MITgcm. In E. Chassignet, A. Pascual, J. Tintoré, & J. Verron (Eds.), *New Frontiers in Operational Oceanography* (pp. 307–392). GODAE OceanView.

Fox-Kemper, B., & Menemenlis, D. (2008). Can large eddy simulation techniques improve mesoscale rich ocean models? *Washington DC American Geophysical Union Geophysical Monograph Series*, *177*, 319–337.

Large, W. G., McWilliams, J. C., & Doney, S. C. (1994). Oceanic vertical mixing: A review and a model with a nonlocal boundary layer parameterization. *Reviews of Geophysics*, *32*(4), 363–403.

Large, W. G., & Yeager, S. G. (2004). *Diurnal to decadal global forcing for ocean and sea-ice models: The data sets and flux climatologies* (Tech. Rep.). University Corporation for Atmospheric Research. Retrieved from `http://dx.doi.org/10.5065/D6KK98Q6`

Leaman, K. D., & Sanford, T. B. (1975). Vertical energy propagation of inertial waves: A vector spectral analysis of velocity profiles. *Journal of Geophysical Research*, *80*(15), 1975–1978.

Losch, M., Menemenlis, D., Campin, J.-M., Heimbach, P., & Hill, C. (2010). On the formulation of sea-ice models. Part 1: Effects of different solver implementations and parameterizations. *Ocean Modelling*, *33*(1-2), 129–144.

Marshall, J., Adcroft, A., Hill, C., Perelman, L., & Heisey, C. (1997). A finite-volume,

incompressible Navier Stokes model for studies of the ocean on parallel computers. *Journal of Geophysical Research: Oceans*, *102*(C3), 5753–5766.

Menemenlis, D., Campin, J.-M., Heimbach, P., Hill, C., Lee, T., Nguyen, A., . . . Zhang, H. (2008). ECCO2: High resolution global ocean and sea ice data synthesis. *Mercator Ocean Quarterly Newsletter*, *31*(October), 13–21.

Rocha, C. B., Chereskin, T. K., Gille, S. T., & Menemenlis, D. (2016). Mesoscale to sub-mesoscale wavenumber spectra in Drake Passage. *Journal of Physical Oceanography*, *46*(2), 601–620.

Savage, A. C., Arbic, B. K., Alford, M. H., Ansong, J. K., Farrar, J. T., Menemenlis, D., . . . others (2017). Spectral decomposition of internal gravity wave sea surface height in global models. *Journal of Geophysical Research: Oceans*, *122*(10), 7803–7821.

Smith, W. H., & Sandwell, D. T. (1997). Global sea floor topography from satellite altimetry and ship depth soundings. *Science*, *277*(5334), 1956–1962.

Welch, P. (1967). The use of fast Fourier transform for the estimation of power spectra: a method based on time averaging over short, modified periodograms. *IEEE Transactions on Audio and Electroacoustics*, *15*(2), 70–73.
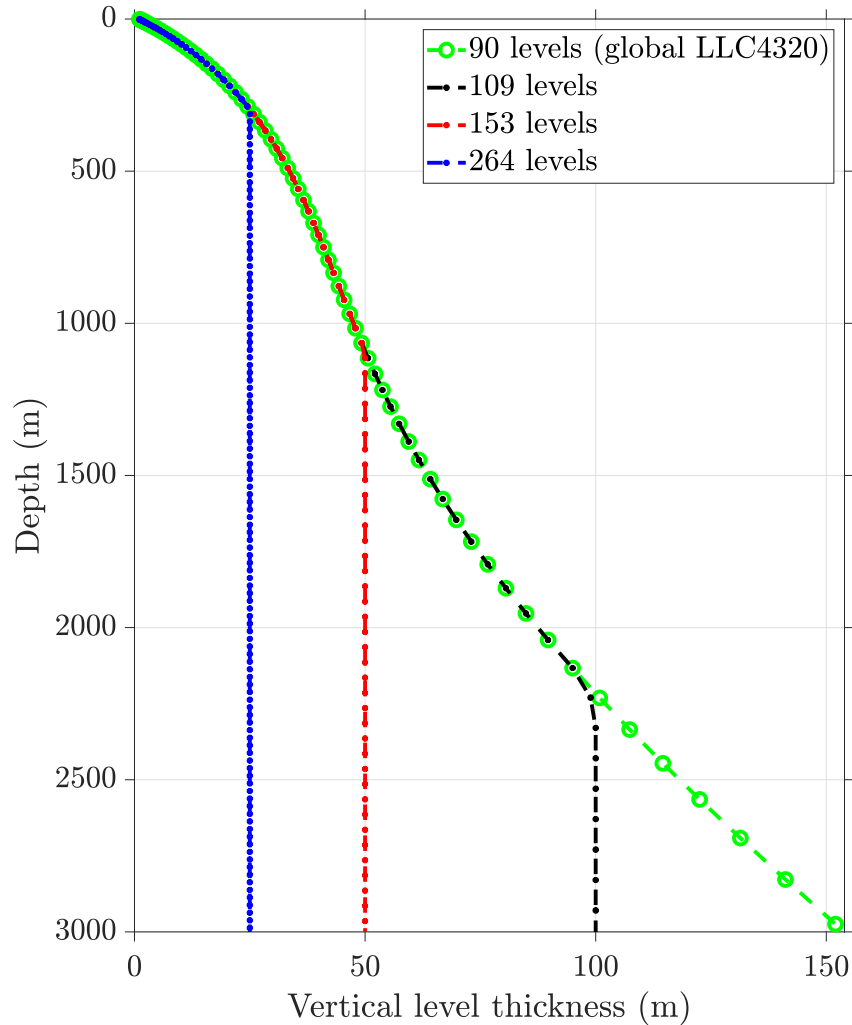
Figure S1. Model vertical level thickness is plotted against ocean depth for the 109-level (black curve with dots), 153-level (red curve with dots), and 264-level (blue curve with dots) regional MITgcm simulations. The vertical level thickness of the global LLC4320 simulation are shown with the green curve with circles. All have the same horizontal grid spacing of 1/48°. The model depth is >6000m at this location but only the upper 3000m are shown.
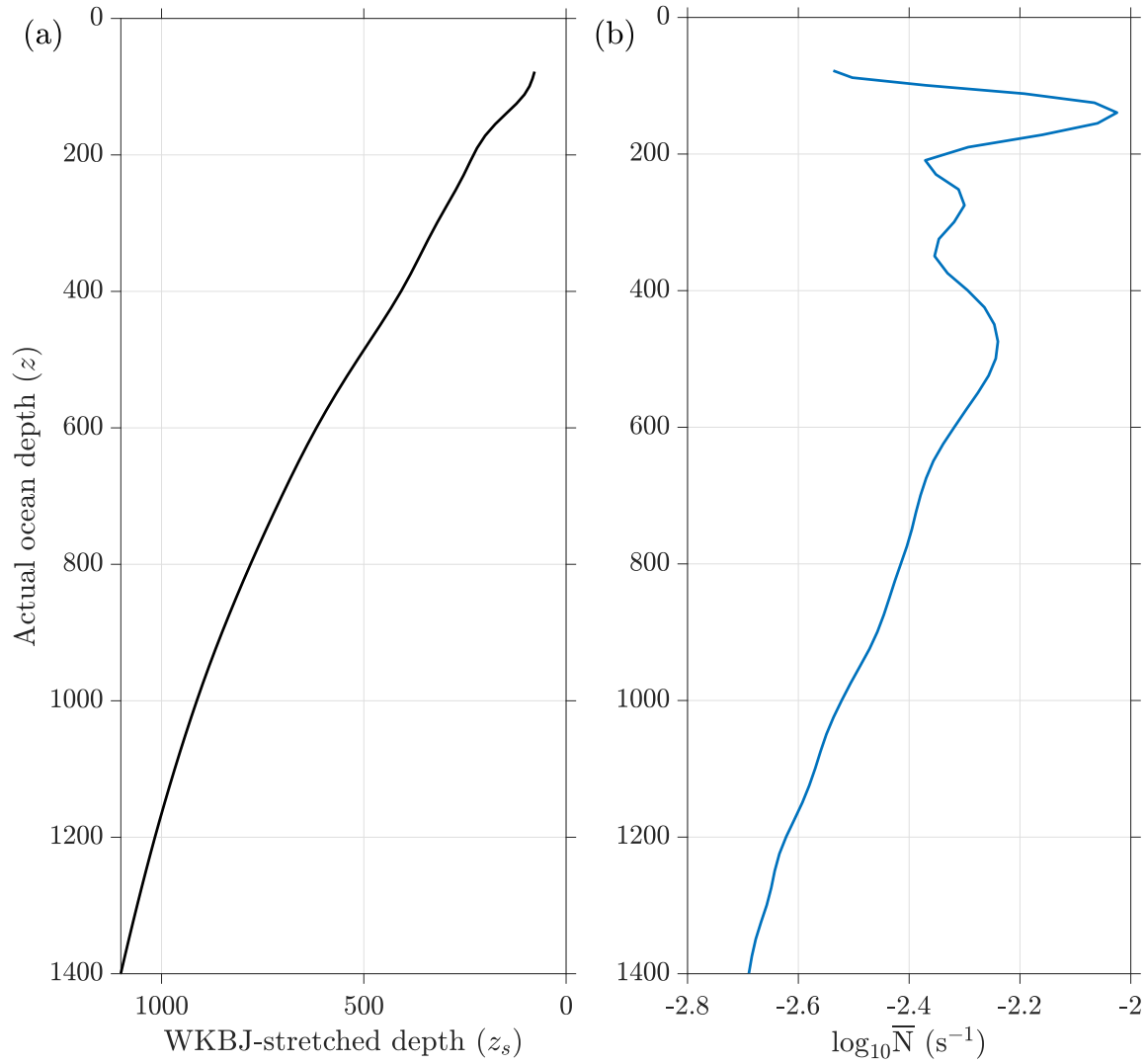
July 16, 2022, 11:13am

Figure S2.   (a) WKBJ-stretched or buoyancy-frequency-stretched depth (z_s) is plotted against actual ocean depth (z) from the 264-level regional simulation at the MP4 location. Despite being from a different year, MP observations have a similar stretched depth vs. actual depth relationship at this location. All vertical wavenumbers calculated in this paper are based on stretched depths. (b) Vertical profile of the logarithm of the time-averaged buoyancy frequency $\overline{N}(z)$ from the same simulation. Only 80–1400m of actual ocean depth from the simulation is shown here because all spectra in the main paper are calculated in this depth range.
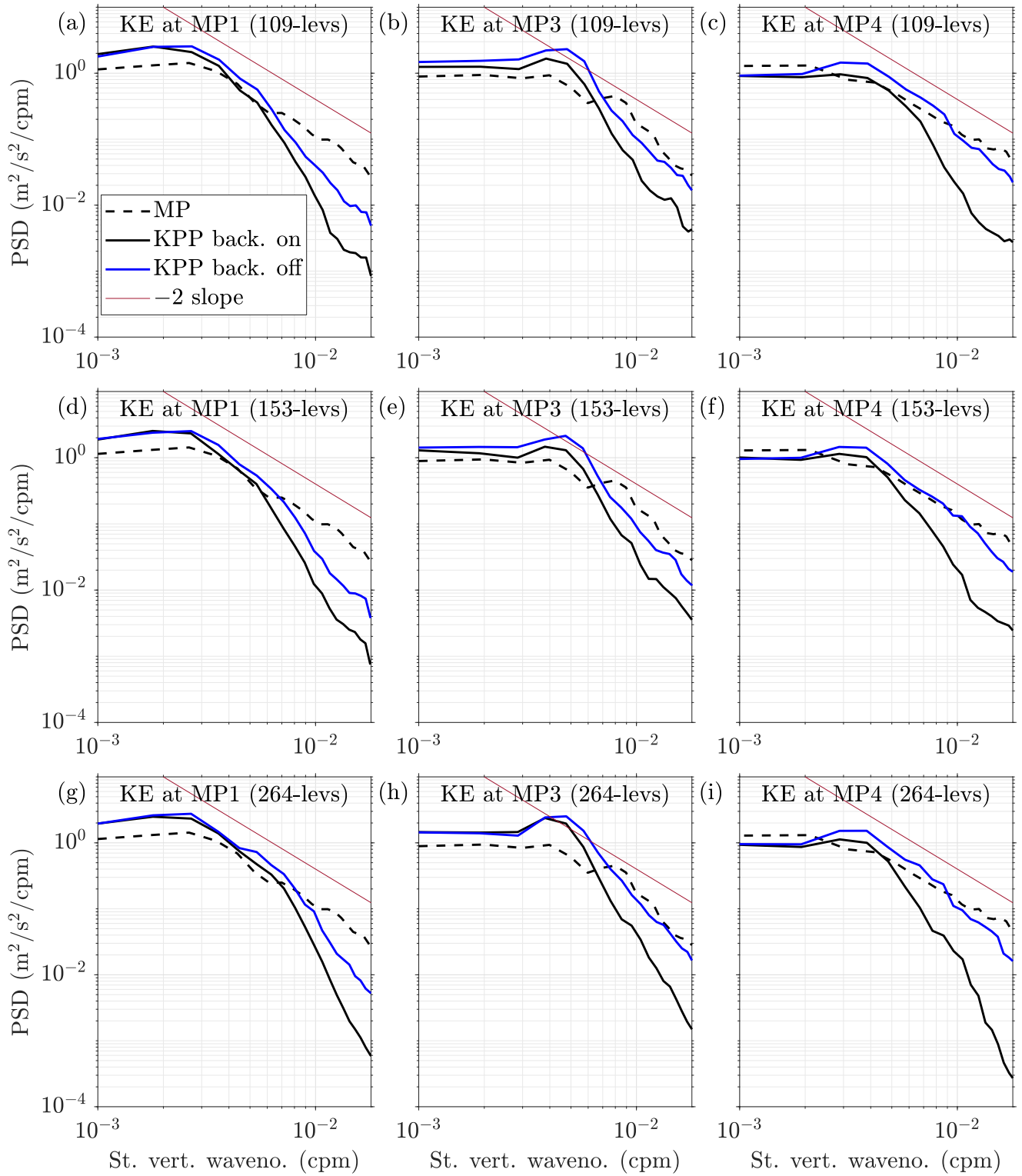
Figure S3. (Caption on next page)

July 16, 2022, 11:13am

Figure S3.   (Previous page) Vertical wavenumber spectra of modeled KE (solid curves) for simulations with (a–c) 109 levels, (d–f) 153 levels, and (g–i) 264 levels, and with the background diffusivity and viscosity components of KPP turned on and off, at different locations as marked in Fig 1 (b) of the main paper are compared to observation (MP) KE spectra. The blue curves represent modeled KE spectra with the KPP background diffusivity and viscosity turned off, while the solid black curves represent modeled KE spectra with the KPP background viscosity set to $\mathcal{O}(10^{-4})$ $\mathrm{m^2s^{-1}}$ in the momentum equations and KPP background diffusivity set to $\mathcal{O}(10^{-7})$ $\mathrm{m^2s^{-1}}$ in the scalar equations which are also same as that of the global model. MP KE spectra are shown in black dashed curves in each. Modeled KE spectra are calculated in the depth range of 80–1400m while the MP KE spectra are calculated in the depth range of 85–1384m. The GM76 KE spectral slope of -2 is plotted in each for reference. The legends for all the subplots are in (a).
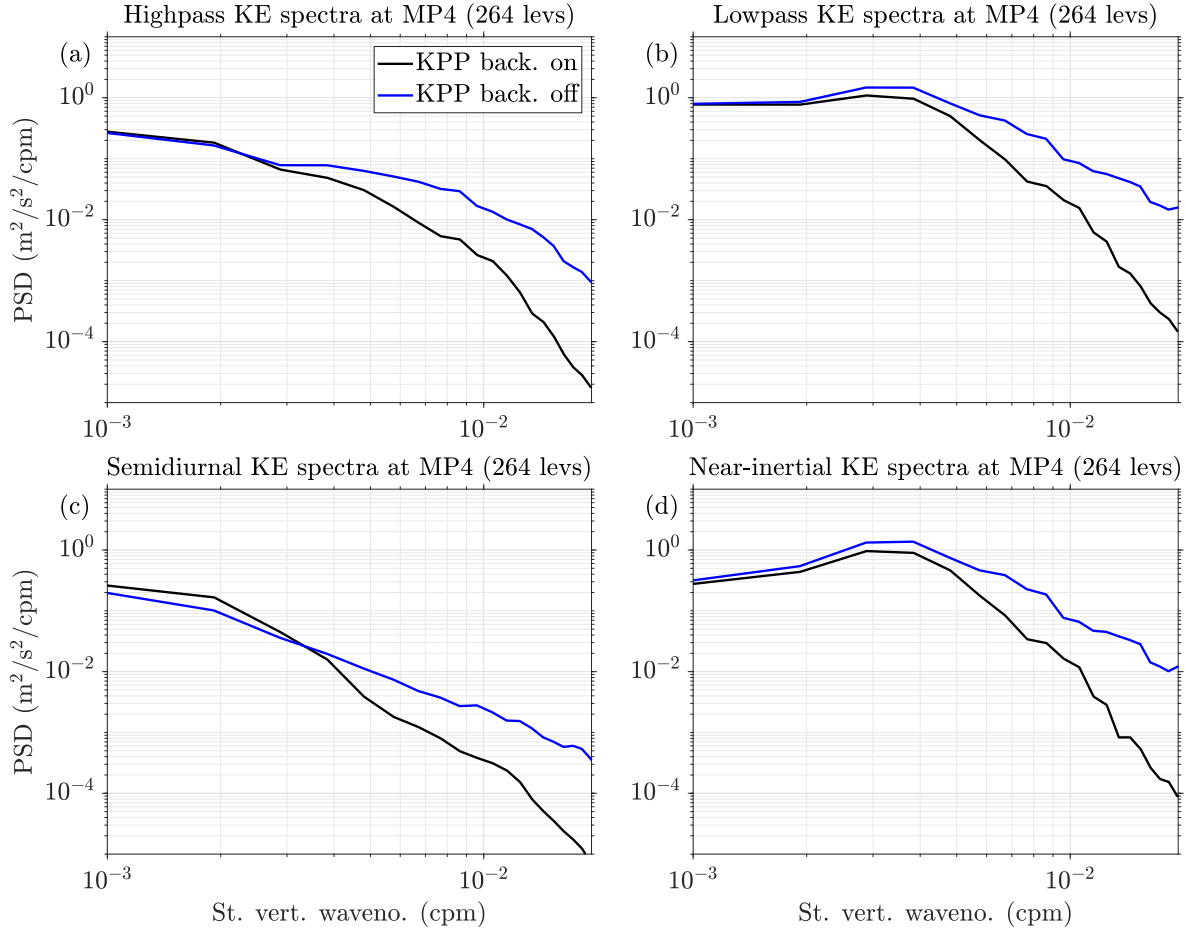
Figure S4. Effect of KPP background on the vertical wavenumber spectra of modeled KE at the MP4 location for the highest-resolution (264-level) simulation in the (a) highpass or supertidal (>11.5 hr), (b) lowpass (<11.5 hr), (c) semidiurnal (11.5–13.5 hr), and (d) near-inertial (90–110% of 23.92 hr) frequency bands. These spectra are calculated in the depth range of 80–1400m. The modeled KE spectra with the KPP background turned off (blue curves) have increased high-wavenumber variance in all the frequency bands when compared to the KE spectra with the KPP background kept on (black curves).
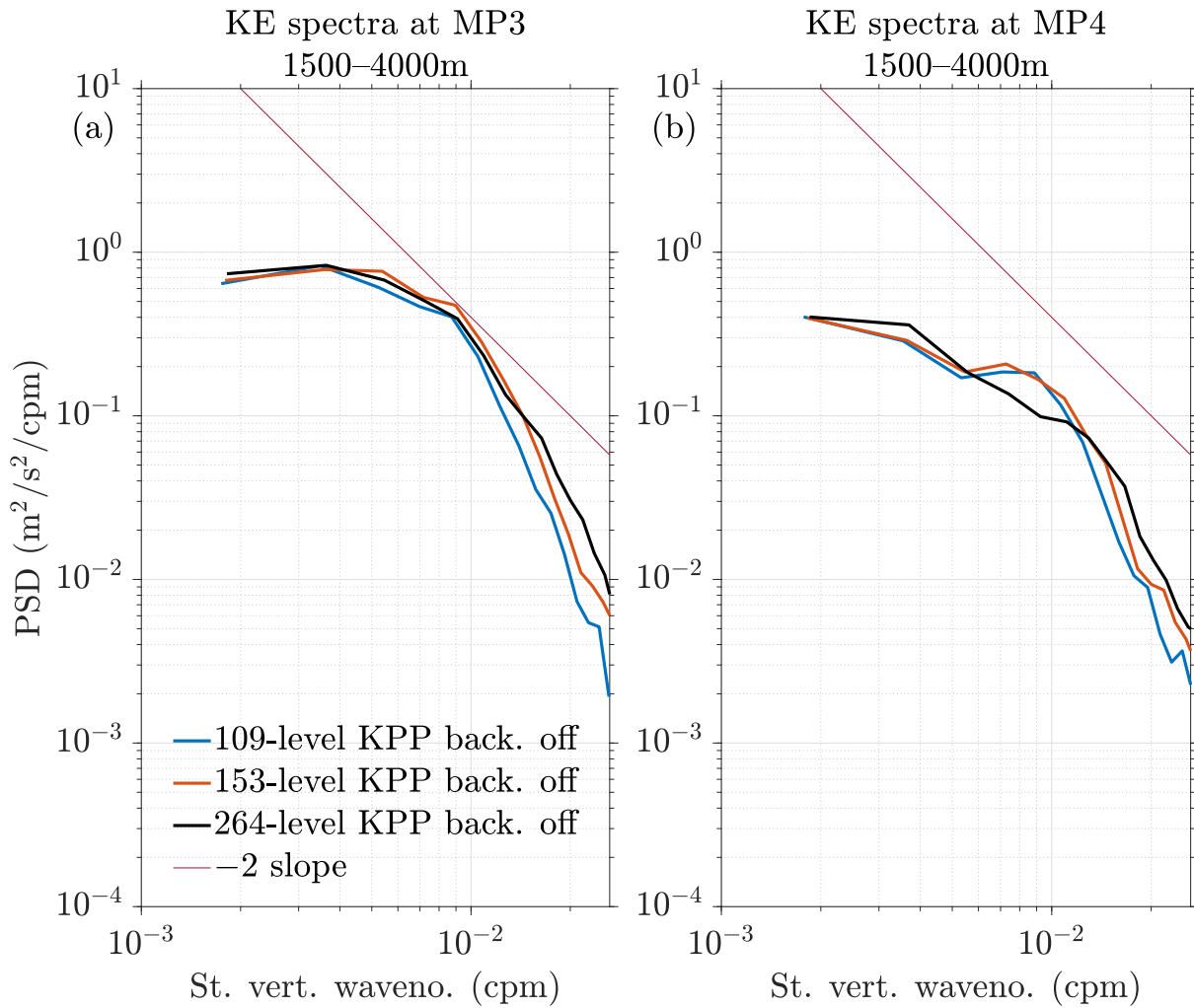
Figure S5.   Vertical wavenumber spectra of modeled KE in the deep ocean (1500–4000m) demonstrate the improvement of the high-wavenumber internal wave continuum with an increase in model vertical resolution at (a) MP3 and (b) MP4 locations. There are no MP measurements in this depth range to compare the modeled spectra with observational spectra. The GM76 KE spectral slope of −2 is plotted in each for reference. The legends for both subplots are in (a).
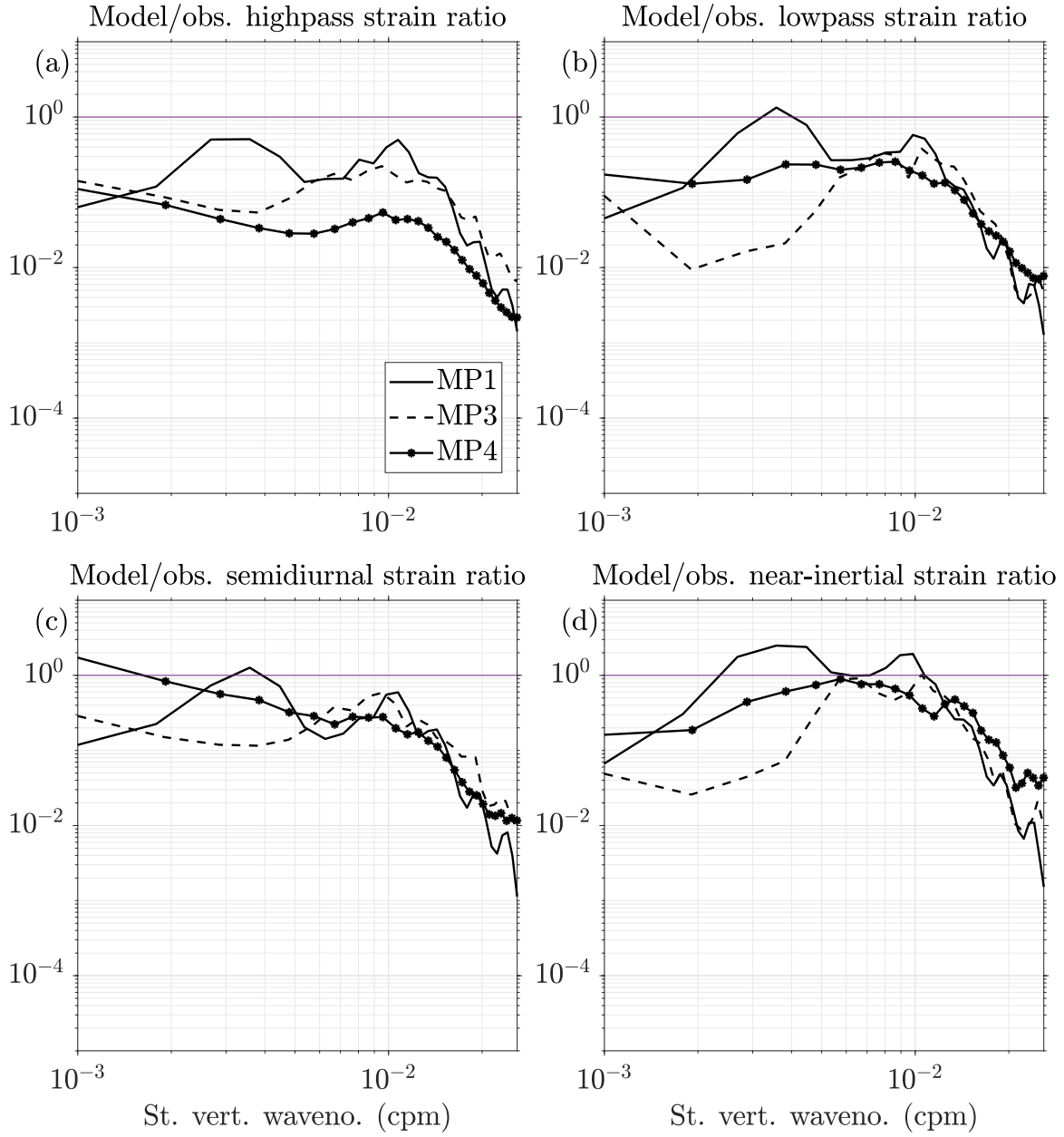
Figure S6. The ratio of strain $(\mathrm{N}^2 - \overline{\mathrm{N}^2})/\overline{\mathrm{N}^2}$ from the 264-level simulation in the depth range of 80–1400m with the KPP background turned off and from MP observations at MP1, MP3, and MP4 in different frequency bands as described in Fig S4. The legends for all the subplots are in (a). Extra horizontal lines are drawn at values of unity for reference.
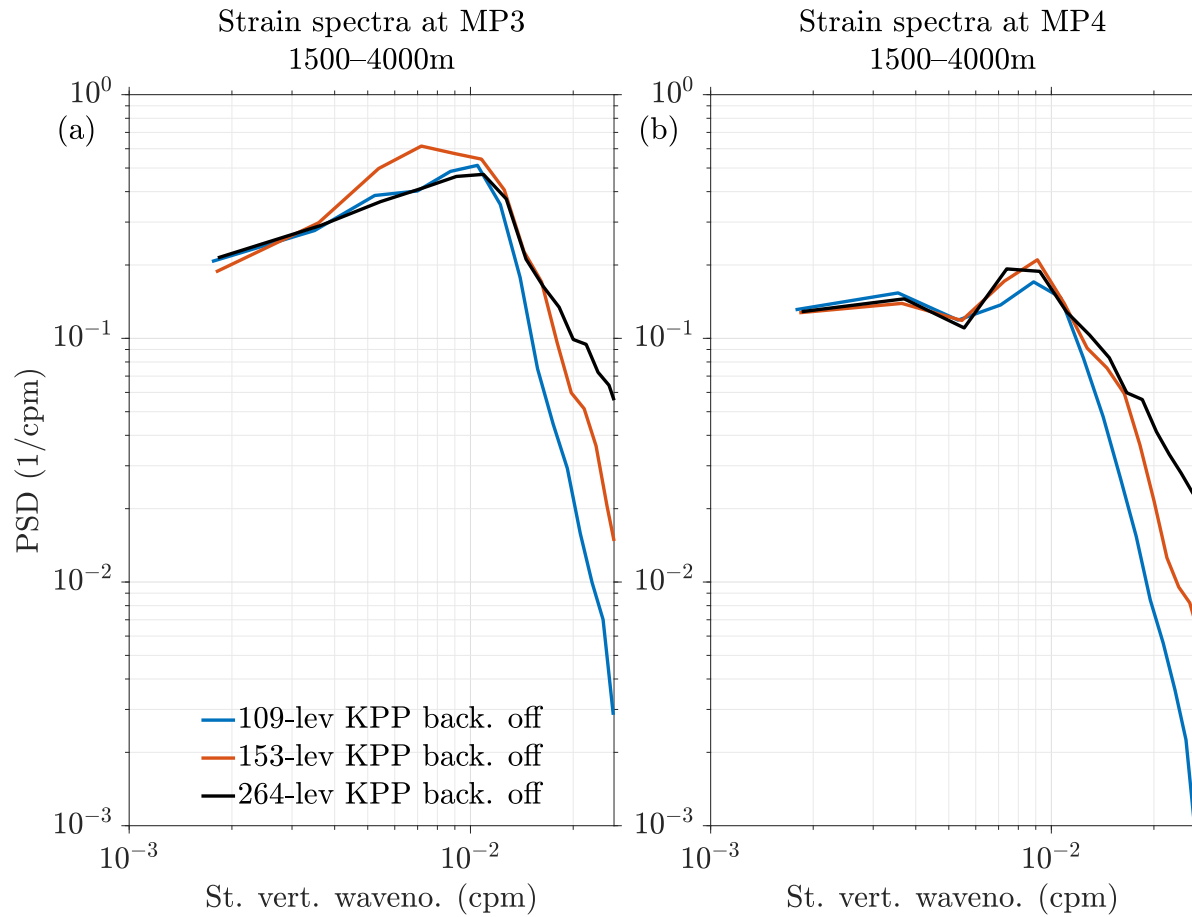
Figure S7.   Vertical wavenumber spectra of modeled strain in the deep ocean (1500–4000m) demonstrate the improvement of strain variance in the internal wave continuum with an increase in model vertical resolution at (a) MP3 and (b) MP4 locations. All spectra are from simulations with the KPP background turned off. The legends for both subplots are in (a).
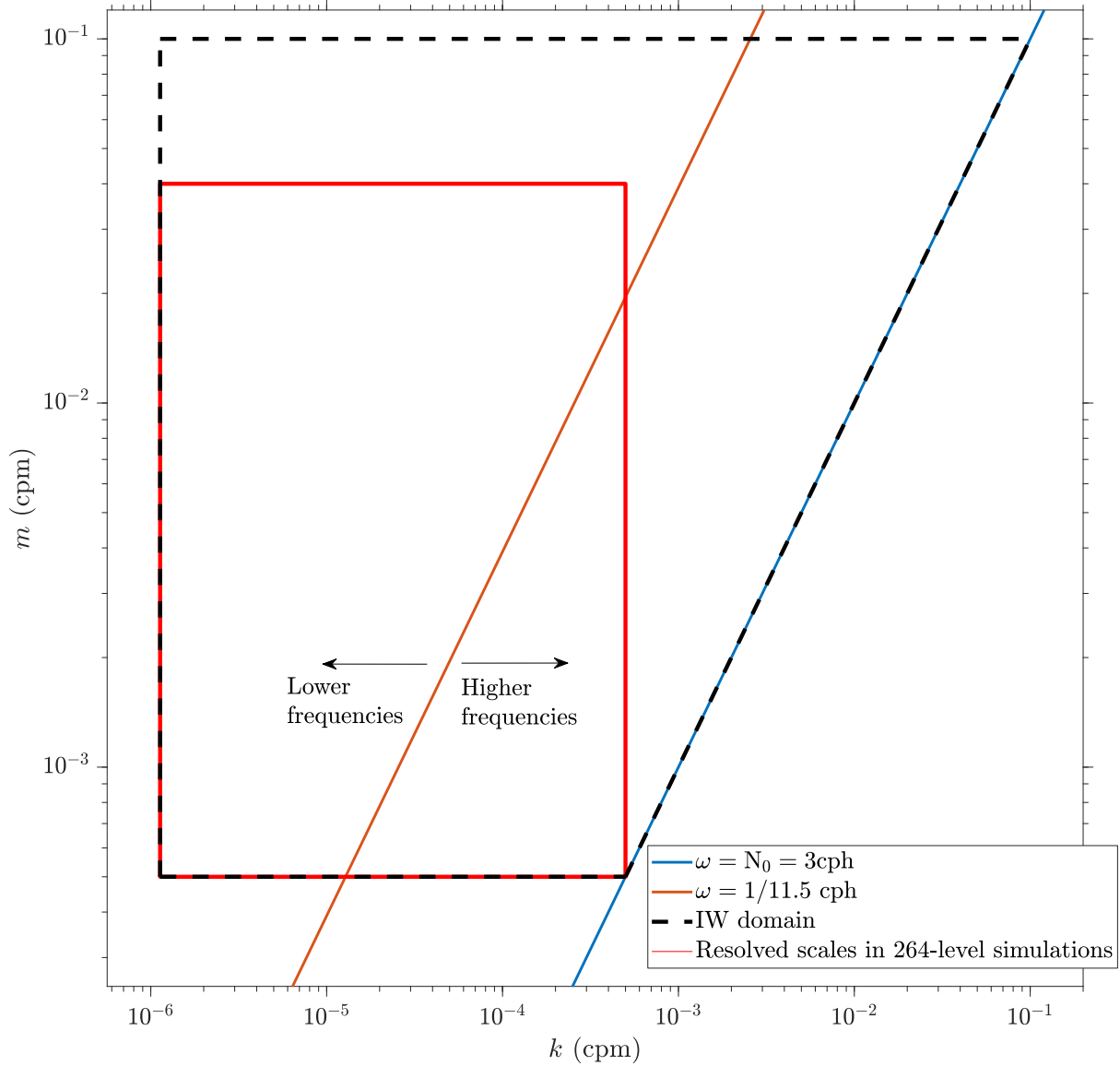
July 16, 2022, 11:13am

Figure S8. The approximate span of the ocean internal wave field is shown by the black dashed lines in a log-log plot of horizontal (k) and vertical (m) wavenumbers. The resolved internal wave scales in the 264-level simulation are bound by the red rectangle. The blue and orange lines are the internal wave dispersion relations at a constant frequency ω. The blue line is for $\omega = N_0 = 3$ cph. The orange line is for $\omega = 1/11.5$ cph that demarcates the highpass (supertidal) and lowpass (subtidal) frequency bands. This figure is a variation of a diagram suggested by an anonymous reviewer.